# Devolatilization of African Palm (*Elaeis guineensis*) Husk Catalyzed by Ferrous Sulfate Studied by TG-MS

## Devolatilización del cuesco de palma (*Elaeis Guineensis*) catalizado con sulfato ferroso estudiado por TG-MS

Alberto R. Albis-Arrieta [1], María C. Romero-Castilla [2], Ever Ortiz-Muñoz [3], Ismael E. Piñeres-Ariza [4], and Edgar F. Donado-Medina [3]

**ABSTRACT**

By means of a thermogravimetric analysis coupled with mass spectroscopy, the catalytic effect of ferrous sulfate on the pyrolysis of African Palm husk (APH) was studied. Thermogravimetric data were adjusted to the distributed activation energy model (DAEM) with four pseudo-components. Ferrous sulfate had a strong influence on the decomposition parameters of the second and fourth pseudo-components of the DAEM, which are identified as hemicellulose and lignin, respectively. The profiles of the signal intensity curves for the selected m/z ratios were successfully modeled using the kinetic parameters obtained by adjusting the thermogravimetric data. It was found that ferrous sulfate promotes the formation of fragments of m/z = 64, 95, and 96, corresponding to molecules, such as $SO_2$, hydrocarbon ions of general formula $[CnH2n-3]+$, and furfural, respectively.

**Keywords:** TG-MS, catalytic pyrolysis, ferrous sulfate, African Palm husk

**RESUMEN**

Mediante el análisis termogravimétrico acoplado a espectroscopía de masas, se estudió el efecto catalítico del sulfato ferroso sobre pirólisis del cuesco de Palma Africana (APH). Los datos termogravimétricos se ajustaron al modelo de energía de activación distribuida (DAEM, por sus siglas en inglés) con cuatro pseudocomponentes. El sulfato ferroso tuvo una fuerte influencia en los parámetros de descomposición del segundo y cuarto pseudocomponente del DAEM, que se identifican como hemicelulosa y lignina respectivamente. Los perfiles de las curvas de intensidad de la señal para las relaciones m/z seleccionadas se modelaron con éxito utilizando los parámetros cinéticos obtenidos del ajuste de los datos termogravimétricos. Se encontró que el sulfato ferroso promueve la formación de fragmentos de m/z = 64, 95 y 96, que corresponden a moléculas como $SO_2$, iones hidrocarburos de fórmula general $[CnH2n-3]+$ y furfural respectivamente.

**Palabras clave:** TG-MS, pirólisis catalítica, sulfato ferroso, cuesco de Palma Africana

## Introduction

Global energy consumption has increased considerably in recent years due to the substantial growth of the global population and industrial development. As a result, the demand for transportation fuels has significantly increased (Bhoi *et al.*, 2020). The development of renewable energy has played an important role in meeting demands and mitigating the dependence on fossil fuels, as they are non-renewable and unsustainable and their use increases the emissions of greenhouse gases (GHG) into the atmosphere, which causes global climate change. Residual biomass has great potential for use in the synthesis of renewable energies because it is found in large quantities, it is available and cheap, and it is ecological and sustainable (Rasid *et al.*, 2020).

Several mechanisms exist through which biomass can be converted into renewable energy sources, such as gasification to produce gaseous fuels or pyrolysis or hydrothermal liquefaction to generate liquid fuels. Pyrolysis can be carried out at ambient pressure. As a result, biomass transformation

[1] Chemical engineer, Universidad Nacional de Colombia, Colombia. Dr. Sc. Chemistry, Universidad Nacional de Colombia, Colombia. Affiliation: Associate Professor, Universidad del Atlántico, Colombia. E-mail: albertoalbis@uniatlantico.edu.co

[2] Chemical engineer, Universidad del Atlántico. E-mail: mceciliaromero@mail.uniatlantico.edu.co

[3] Physics graduate, Universidad Pedagógica de Colombia, Colombia. M.Sc. Physics, Universidad del Valle, Colombia. Dr.Sc. Physics, Universidad del Valle, Colombia. Affiliation: Full Professor, Universidad del Atlántico, Colombia. E-mail: everortiz@uniatlantico.edu.co

[4] Physics graduate, Universidad del Atlántico, Colombia. M.Sc. Physics, Universidad del Atlántico, Dr.Sc. Physics, Universidad del Atlántico, Colombia. Affiliation: Assistant Professor, Universidad del Atlántico, Colombia. E-mail: ismaelpineres@mail.uniatlantico.edu.co

[5] Chemical Engineer, Universidad del Atlántico. E-mail: edgardonado@ingenieros.com.

into liquid fuels through pyrolysis has become very attractive (Hu and Gholizadeh, 2019). Pyrolysis is the thermochemical decomposition of biomass in the absence of oxygen at temperatures between 300 and 700 ˚C. From this process, liquid bio-oil, non-condensable gases, and solid biochar are obtained (Brassard et al., 2017). Non-condensable gases can be used to provide energy to the pyrolysis process. Catalytic Fast Pyrolysis (CFP) is commonly used to transform biomass into high-quality bio-oil, deoxygenating the $H_2O$, $CO$, and $CO_2$ vapors formed during the process (Chen et al., 2019).

Oil palm (Elaeis guineensis) is the world's main source of vegetable oil, and it is produced principally by Malaysia and Indonesia. Oil palm industry residues constitute the biggest source of biomass in Malaysia, produced in large quantities throughout the year, but only a small fraction is converted into value-added products. Colombia is the second largest producer outside Southeast Asia and the largest producer in South and Central America (Onoja et al., 2019; Rivera-Méndez et al., 2017). African Palm Husk (APH) is produced as a result of the extraction of palm oil and is a biomass available in large quantities to be transformed. Many efforts have been made to take advantage of solid waste from the palm oil industry. Some studies involve the pyrolysis of this biomass using TG-MS, catalytic pyrolysis with low-cost catalysts, conversion of oil palm biomass to hydrogen via gasification reaction in supercritical water, metal oxide-catalyzed hydrothermal liquefaction of oil palm biomass, among others (Salema et al., 2019; Ro et al., 2018; Kelly-Yong et al., 2007; Yim et al., 2017).

It has become essential to know the effect of heavy metals as catalysts in the pyrolysis of metal-impregnated biomass, as well as their distribution in pyrolysis products, in order to find a suitable way of using them (Han et al., 2018). The effect of metallic salts as catalysts in this process has been studied by several authors (Zhao et al., 2017; Cao et al., 2020). Moreover, metal (Ru/Fe) impregnated banana pseudo-stem (Kumar et al., 2019), and copper and iron salts as additives in wood pyrolysis (Edye et al., 1992) have been studied.

Due to its advantages, biomass has gained interest as a green renewable energy. Lignocellulosic biomass is composed of cellulose (32-45%), hemicellulose (19-25%), and lignin (14-26%), which usually makes for very complex thermal decomposition profiles (Kaur et al., 2018; Han et al., 2018). The combination of thermogravimetric analysis coupled with mass spectrometry (TGA-MS) appears to provide a deeper insight into the identification and quantification of devolatilization products. One of the main advantages of TGA-MS is that it can afford real-time and sensitive detection of evolved gases, which is an important and often difficult task in many thermal applications (Malika et al., 2016).

In this work, the effect of $FeSO_4$ as a catalyst on the devolatilization kinetics of APH and its product distribution at 10 and 100 K/min heating rates were studied using the TG-MS simultaneous analysis technique, as a continuation of a previous study on APH devolatilization by TG-MS in the absence of a catalyst (Albis et al., 2018). Kinetics parameters obtained using TGA were fitted to the Distributed Activation Energy Model (DAEM).

## Methodology

### Materials

The APH was obtained from a biodiesel plant in the municipality of Santa Marta, Magdalena, Colombia. Biomass was ground (particle size < 200 mm) and stored in a desiccator for further use.

### Sample preparation

An aqueous solution of $FeSO_4$ was prepared by dissolving 2 000 g of the salt at 75% in 100 ml of water to obtain a final concentration of 15 mg Fe/ml. The prepared APH was added to the solution in the adequate volume, and the suspension was stirred for 2 h. Then, the sample was dried at 80 ˚C for 2 h, and thereafter for 2 h at 105 ˚C. The final concentration of $FeSO_4$ in the biomass was 1,5% by weight.

### Thermogravimetric Analysis (TGA)

Thermogravimetric analysis was performed using a TA instruments TGA 2950 thermogravimetric analyzer. Control and acquisition of experimental data were carried out via the Universal Analysis software. The procedure for this analysis was the same as that used in the previous study (Albis et al., 2018).

### Distributed Activation Energy Model

The DAEM is a multiple reaction model widely used in the pyrolysis of lignocellulosic biomass. This model assumes that the decomposition mechanism takes a large number of independent, parallel, first-order, or $n^{th}$-order reactions with different activation energies, reflecting variations in species' bond strengths. The difference in activation energies can be represented by a continuous distribution function (Cai et al., 2014). As described in Albis et al. (2018), in this model, the mass conversion rate is represented by several numbers of reactions that share the same frequency factor $(A_j)$, with an activation energy distributed in Gaussian form. A media activation energy $E_{0j}$ and a standard deviation of the activation energy $(\sigma_j)$ are part of the model represented by Equations (1) and (2).

$$Y^{calc}(t) = -\sum_{j=1}^{M} c_j \frac{dx_j}{dt} \qquad (1)$$

Where, according to Albis et al. (2018):

$Y^{calc}$ represents the conversion rate of the sample or signal strength, $M$ is the number of reactions or pseudo-

components of the sample, $c_j$ is a proportionality constant, $x_j$ is the unreacted fraction of the material represented by the $j$-th kinetic equation, and $\frac{dx_j}{dt}$ is the rate of production or consumption of $j$, which can be calculated as:

$$\frac{dx_j}{dt}(t) = \frac{1}{2\sqrt{\pi}} \int_{-\infty}^{\infty} exp\left[\mu_j^2\right] exp\left[0,75\left|\left|\mu_j^2\right|\right]\frac{dx_j\left(t,\mu_j\right)}{dt}d\mu_j \quad (2)$$

where $\mu_j = 2\left(E - E_{0j}\right)/\left(\sqrt{2}\sigma_j\right)$ and $X_j\left(t,\mu_j\right)$ are the solution for $dx_j/dt$ at time $t$, and the value of the energy of activation is $E$.

Equation (2) was solved using MATLAB, as described by Albis *et al.* (2014).

## Results

### Thermogravimetric Analysis (TGA)

The TG and DTG of the samples of APH and APH + 1% FeSO$_4$ at temperature rates of 10 and 100 K/min are shown in Figures 1a and 1b, respectively. In Figure 1, four events are observed: the first is related with water release at temperatures below 393 K; the second, at temperatures between 393 and 475 K, which approximately corresponds to the first thermal decomposition; followed by the main pyrolytic event, which shows two peaks; and, finally, the last event is a slow-rate decomposition.

In Figure 1a, a displacement to the right with increased heating rate from 10 to 100 K/min is noted in the thermogram in both cases, *i.e.*, in the absence and presence of the catalyst, related to a small increase in sample weight loss. A similar percentage of char reported in the absence of the catalyst (Albis *et al.*, 2018) was also observed in its presence, which is within the limits of experimental uncertainty. This means that the presence of the catalyst does not affect the percentage of carbonization at either of the two heating rates evaluated.

In the main pyrolytic event, the first peak is associated with hemicellulose decomposition, and the second one with the disintegration of cellulose. In Figure 1b, a difference in the formation of peaks in the presence of FeSO$_4$ is observed, which is related to an increase in the second pseudo-component (corresponding to hemicellulose) within the DTG peak. This peak is higher in the pyrolytic event than the hemicellulose peak for the APH pyrolysis in the absence of the catalyst at the heating rates studied.

The presence of FeSO$_4$ leads to a hemicellulose reduction in the DTG peak temperature at heating rates of 10 and 100 K/min. This behavior suggests a catalytic effect that causes the pyrolytic process to start earlier. In previous studies, it was found that the promoting effects of FeSO$_4$ were noticeable in the hydrolysis of microcrystalline cellulose –an 84,14% conversion was obtained. It was also found that

the depolymerization and hydrolysis of biomass remains active in the presence of metals that lower the degradation temperature of the biomass (Tao *et al.*, 2010). This shows the capability of catalysts of initiating pyrolysis reactions at lower temperatures.
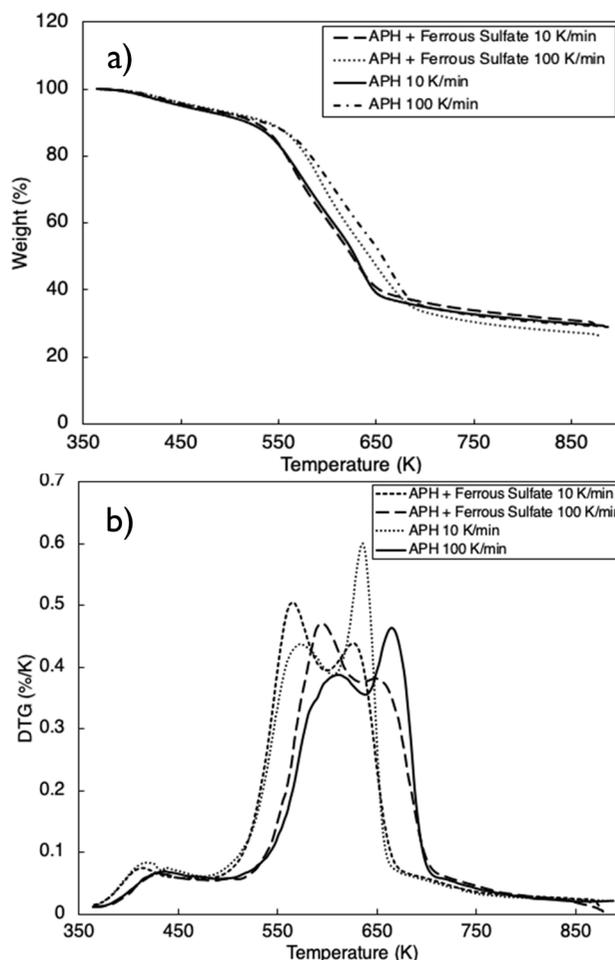


**Figure 1.** a) TG and b) DTG thermograms of APH and APH + 1% FeSO$_4$ at heating rates of 10 and 100 K/min, respectively
**Source:** Authors

### Fitting to the DAEM

In Figure 2, the fitting of the DAEM in the presence of the catalyst at heating rates of 10 and 100 K/min is shown. Given the number of peaks, Figure 1b suggests the use of at least four pseudo-components. Consequently, the DAEM with four pseudo-components is used to illustrate the experimental data in this study.

The fitting of the data regarding the conversion rate to the DAEM with four pseudo-components for pyrolysis of APH with FeSO$_4$ heated at 10 and 100 K/min is shown in Table 1. In comparison with a previous study (Albis *et al.*, 2018), the results in Table 1 show that the catalytic effect of FeSO$_4$ affects mainly the second and fourth pseudo-components, identified as hemicellulose and lignin, reducing their average activation energies and their corresponding standard deviations. This behavior explains the reduced starting

temperature for the pyrolysis process of APH in the presence of a catalyst: reduction of the activation energy increases the decomposition rate of these compounds, and reduction in the standard deviations of the activation energy causes these components to have a narrow temperature range. For the third pseudo-component, identified as cellulose, the catalytic effect of $FeSO_4$ enhances the standard deviation of the activation energy, which produces a broad temperature range. Moreover, the proportionality constant decreased for the first, second, and third pseudo-components, but increased for the fourth one. On the other hand, the values of the frequency factors remained within the range of values reported for all pseudo-components. Prior studies have reported the catalytic effects of $FeSO_4$ in the decomposition of lignin in wood pyrolysis (Edye et al., 1992), as well as the catalytic effects of ferric sulfate in hemicellulose pyrolysis (Albis et al., 2018).
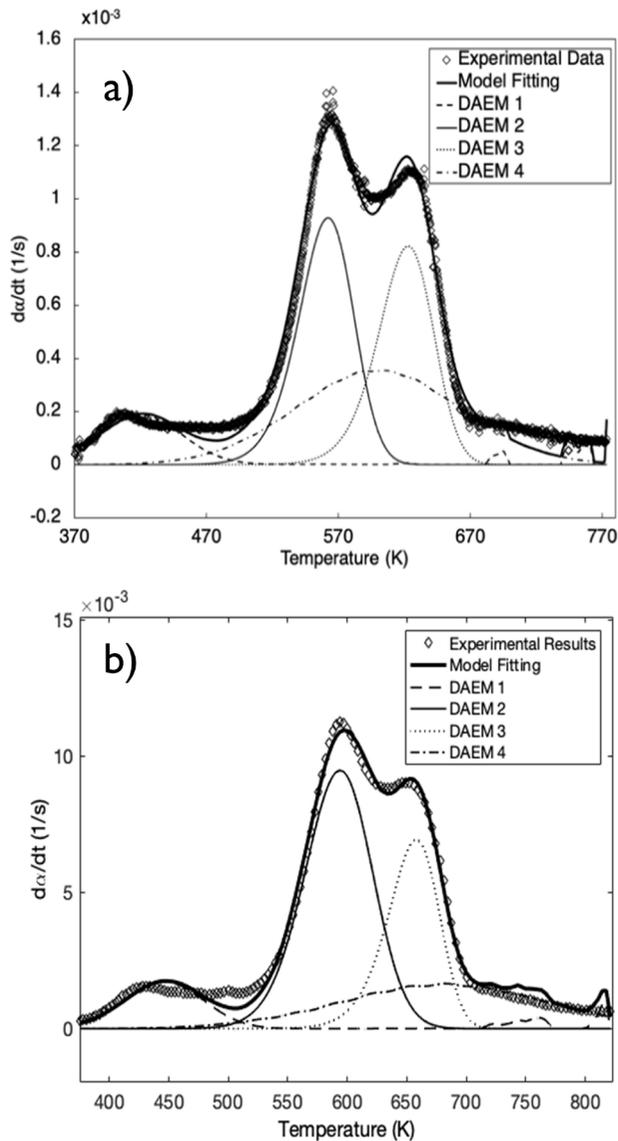
**Table 1.** DAEM parameters with four pseudo-components for APH + 1,5% $FeSO_4$ at heating rates of 10 and 100 K/min

| DAEM Parameter | Heating Rates | |
| :---: | :---: | :---: |
| | $\beta$ = 10 K/min | $\beta$ = 100 K/min |
| $C_1$ | 0,166 | 0,179 |
| $A_1$ | 1,270E+15 | 1,270E+15 |
| $E_{01}$ | 1,380E+05 | 1,380E+05 |
| $S_1$ | 1,900E+04 | 1,900E+04 |
| $C_2$ | 5,767E-01 | 6,864E-01 |
| $A_2$ | 1,274E+14 | 1,274E+14 |
| $E_{02}$ | 1,739E+05 | 1,733E+05 |
| $S_2$ | 8,550E+03 | 1,082E+04 |
| $C_3$ | 5,161E-01 | 3,964E-01 |
| $A_3$ | 7,987E+14 | 7,987E+14 |
| $E_{03}$ | 2,023E+05 | 2,013E+05 |
| $S_3$ | 8,518E+03 | 6,269E+03 |
| $C_4$ | 6,474E-01 | 6,573E-01 |
| $A_4$ | 1,064E+14 | 1,064E+14 |
| $E_{04}$ | 1,864E+05 | 1,863E+05 |
| $S_4$ | 3,832E+04 | 3,833E+04 |
| SE | 4,359E-05 | 2,396E-04 |

**Source:** Authors





**Figure 2.** Fitting of the DAEM with four pseudo-components for APH + 1% $FeSO_4$ at a) 10 K/min and b) 100 K/min
**Source:** Authors

It was found that, in comparison with the previous study (Albis et al., 2018), the activation energy for the first pseudo-component (Ea = 1,38E+5 kJ/mol), identified as extractives, remained the same in the absence and presence of the catalyst for the heating rates studied. The activation energy for the second pseudo-component, identified as hemicellulose, went from Ea = 1,77E+05 kJ/mol in the absence of the catalyst to Ea = 1,739E+05 kJ/mol and Ea = 1,733E+05 kJ/mol in the presence of $FeSO_4$ at heating rates of 10 and 100 K/min, respectively. Furthermore, the activation energy for the third pseudo-component, identified as cellulose, went from Ea = 2,04E+05 kJ/mol in the absence of the catalyst to Ea = 2,023E+05 kJ/mol and Ea = 2,013E+05 kJ/mol in the presence of $FeSO_4$ at 10 and 100 K/min, respectively. The activation energy for the fourth pseudo-component, identified as lignin, went from Ea = 1,95E + 05 kJ/mol in the absence of the catalyst to Ea = 1,864E+05 kJ / mol and Ea = 1,863E+05 kJ/mol in the presence of $FeSO_4$ at 10 and 100 K/min, respectively. The decreased activation energy shows the catalytic effect of $FeSO_4$ on APH pyrolysis.

A previous study on pyrolysis of banana pseudo-stem found that, in comparison with raw biomass (Ea =116,22 kJ/mol), samples impregnated with $FeSO_4$ have a lower activation energy (Ea = 86,78 kJ/mol). The catalytic effect lowers the activation energy, thus enhancing the reaction rate with modified reaction pathways (Kumar et al., 2019).

**Figure 3.** Fitting of the DAEM with four pseudo-components of selected m/z signal intensities: a) m/z = 32, b) m/z = 34, c) m/z = 44, d) m/z = 50 of APH + 1% $FeSO_4$ at a 10 K/min heating rate
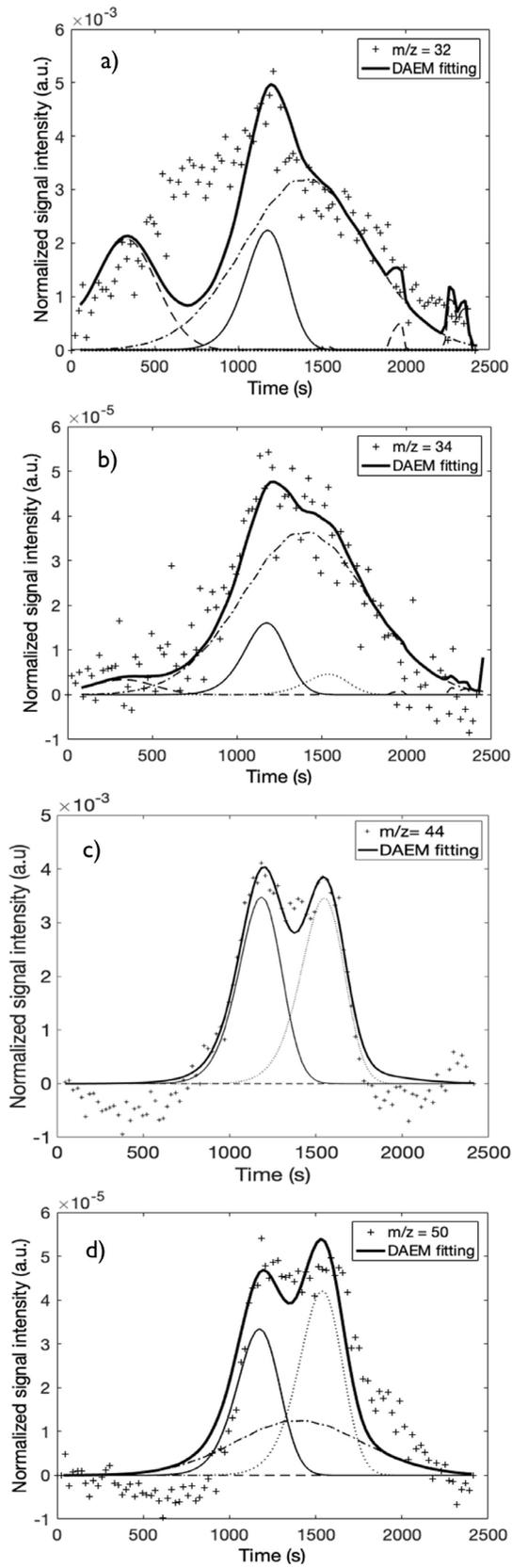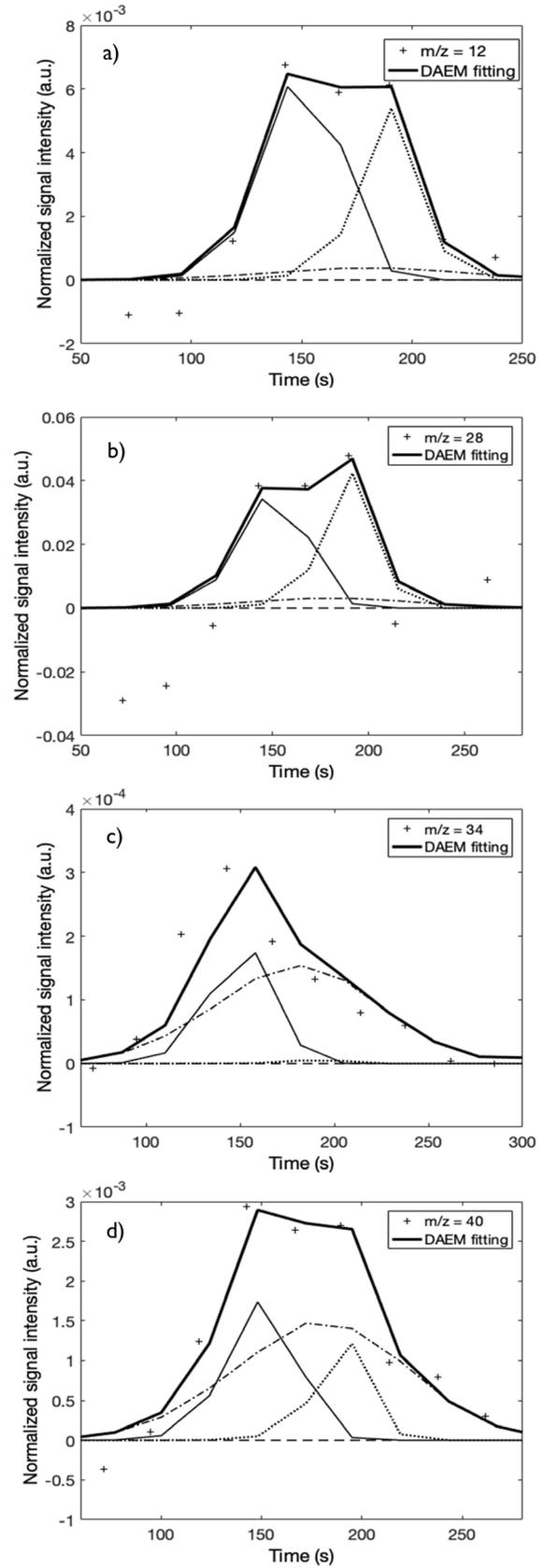**Source:** Authors



**Figure 4.** Fitting of the DAEM with four pseudo-components of selected m/z signal intensities: a) m/z = 12, b) m/z = 28, c) m/z = 34, d) m/z = 40 of APH + 1% $FeSO_4$ at a 100 K/min heating rate
**Source:** Authors

*Mass spectrometry*

Figures 3 and 4 show the fitting of the DAEM with four pseudo-components for some of the m/z ratios at heating rates of 10 and 100 K/min, respectively. The fit for all the m/z curves at the heating rates studied is supplied in the complementary material.

To analyze the effect of the catalyst, the data obtained at the 10-K/min heating rate is used because, due to the high speed, very few points were obtained in the areas of interest at 100 K/min (Figure 4). Table 2 shows the mass spectrometric intensities selected for kinetic evaluation and its presence in the main thermal events at heating rates of 10 and 100 K/min.

At the heating rate of 10 K/min, the fragments associated with m/z = 2, 16, 28, and 40 did not evolve during pyrolysis in the presence of the catalyst. The signal intensities m/z = 12, 14, 17, 32, 34, 44, 50, 51, 55, 58, 60, and 98 for APH pyrolysis in the presence of $FeSO_4$ were lower than the signals corresponding to the absence of the catalyst (Albis *et al.*, 2018). These signals were assigned to methane (m/z =12 and 14), water (m/z = 17), methanol (m/z = 32), hydrogen sulfide (m/z = 34), and carbon dioxide (m/z = 44). The fragments associated with m/z = 50 and 51 were assigned to furfural and benzene. m/z = 55 was assigned to cyclohexanone, 2(5H)-furanone, or 1,4-dimethylcyclohexane, $C_3H3O^+$. m/z = 58 was assigned to isobutane, propanal, acetone, or propanol. m/z = 60 was assigned to acetic acid, dodecanoic acid, hexadecanoic acid, or octadecanoic acid, and m/z = 98 was assigned to 1,2-cyclopentanedione, 4-methyl-5H-furan-2-one, 3-furanmethanol, or cyclohexanone.

In addition, the signal intensities of the m/z = 64, 95, and 96 ratios for APH pyrolysis in the presence of $FeSO_4$ were greater than those corresponding to the absence of the catalyst. This behavior suggests that $FeSO_4$ promotes the formation of these compounds. Signals were assigned to the production of $[SO_2]^+$ or $[SONH_2]^+$ (m/z = 64) (Kuehl and Rozynov, 2003), hydrocarbon ions of general formula $[C_nH_{2n-3}]^+$ (m/z = 95) (Mjøs, 2004), and furfural (m/z = 96) (Shen *et al.*, 2015). It has been reported that Fe, as a catalyst, removes the oxygenated compounds from the pyrolysis process, thus, improving bio-oil quality and, consequently, increasing the formation of hydrocarbons. Also, the aqueous solution contains aldehydes (Kumar *et al.*, 2019; Ansari and Gaikar, 2019).

## Fitting mass spectrometry data to the DAEM

Tables 3 and 4 show the proportionality constant values ($c_i$) for the DAEM with four pseudo-components for the m/z signals detected regarding the pyrolysis of APH + 1% $FeSO_4$ at heating rates of 10 and 100 K/min.

When comparing these results to those of a previous study (Albis *et al.*, 2018), several observations can be made. In the absence of the catalyst, at a heating rate of 10 K/min, the fragments associated with m/z = 12, 17, 18, 60, and 95 were associated with the thermal decomposition of hemicellulose, cellulose, and lignin. However, in the presence of the catalyst, these fragments were associated only with the thermal decomposition of hemicellulose and cellulose, with the contribution of the thermal decomposition of lignin being almost negligible. In the case of the fragments associated with m/z = 51, 55, and 96, the gases evolved were associated with hemicellulose, cellulose, and lignin decomposition with and without the catalyst. For the m/z ratios described, in the absence of the catalyst, the peak corresponding to the decomposition rate of hemicellulose is lower than that corresponding to the decomposition rate of cellulose. In contrast, in the presence of the catalyst, the peak corresponding to the decomposition rate of hemicellulose is higher than that corresponding to the decomposition rate of cellulose. This, except for m/z = 55, whose main event is associated with the thermal decomposition of lignin. This behavior coincides with the results obtained in the DTG curves described.

**Table 2.** m/z obtained for the kinetic study and its presence in the main thermal event at heating rates of 10 and 100 K/min

| m/z | Heating Rate Component/ Fragment-molecule | 10 K/min | | | | 100 K/min | | | |
|---|---|---|---|---|---|---|---|---|---|
| | | E | H | C | L | E | H | C | L |
| 2 | $H_2$ | NA | NA | NA | NA | NA | NA | NA | NA |
| "12 | C | - | + | + | - | - | + | + | + |
| 14 | $CH_4$ | - | + | - | + | - | + | + | + |
| 16 | $CH_4$ | NA | NA | NA | NA | - | - | + | + |
| 17 | $H_2O$ | - | + | + | - | - | + | + | + |
| 18 | $H_2O$ | - | + | + | - | - | + | + | + |
| 28 | CO | NA | NA | NA | NA | - | + | + | + |
| 30 | formaldehyde | NA | NA | NA | NA | - | + | + | + |
| 32 | Methanol | + | + | - | + | + | + | - | + |
| 34 | $H_2S$ | + | + | + | + | - | + | - | + |
| 40 | Furfural | NA | NA | NA | NA | - | + | + | + |
| 42 | Acetonitrile | NA | NA | NA | NA | - | + | + | + |
| 44 | $CO_2$ | - | + | + | - | - | + | + | + |
| 46 | $NO_2$ | NA | NA | NA | NA | + | + | + | + |
| 50 | Furfural; benzene | - | + | + | + | - | + | + | + |
| 51 | Furfural; benzene | - | + | + | + | - | + | + | + |
| 52 | Benzene | - | + | + | + | - | + | + | + |
| 53 | 2-Furanmethanol; 5- Methyl-2-furancarboxaldehyde | - | + | + | + | - | + | + | + |
| 54 | 4,4-dimethylcyclohexene | - | + | + | + | NA | NA | NA | NA |
| 55 | Cyclohexanone; 2(5H)-Furanone; 1,4-Dimethylcyclohexane,C3H3,O+ | - | + | + | + | NA | NA | NA | NA |
| 56 | 4,4-dimethylcyclohexene | - | + | + | + | - | + | + | + |
| 58 | Isobutane, propanal, acetone, propanol | - | + | + | + | - | + | - | + |
| 60 | Acetic acid; dodecanoic acid; hexadecanoic acid; octadecanoic acid | - | + | + | - | - | + | + | + |
| 64 | $[SO2]^+$ or $[SONH2]^+$ | - | + | + | - | - | + | - | + |
| 95 | Hydrocarbon ions of general formula $[C_nH_{2n-3}]^+$ | - | + | + | + | - | + | + | + |
| 96 | Furfural | - | + | + | + | - | + | + | + |
| 98 | 1,2-Cyclopentanedione; 4- Methyl-5H-furan-2-one; 3- Furanmethanol; cyclohexanone | - | + | + | + | - | + | + | + |

E= Extractives ; H= Hemicellulose ; C= Cellulose ; L= Lignin ; NA= Not-Applicable
**Source:** Authors

**Table 3.** Proportionality constants regarding the DAEM with four pseudo-components for m/z signals detected related with the pyrolysis of APH + 1% FeSO$_4$ at a 10 K/min heating rate

| m/z | $c_1$ | $c_2$ | $c_3$ | $c_4$ |
|---|---|---|---|---|
| 2 | 2,293E-01 | 8,275E-07 | 1,842E-01 | 3,901E-01 |
| 12 | 3,787E-07 | 1,657E-01 | 2,273E-01 | 1,078E-01 |
| 14 | 2,755E-07 | 9,183E-01 | 3,570E-02 | 2,531E |
| 16 | 7,661E-08 | 1,509E-02 | 5,647E-02 | 6,413E-02 |
| 17 | 5,532E-08 | 1,270E-01 | 2,035E-01 | 1,331E-01 |
| 18 | 3,526E-06 | 6,935E-01 | 1,085E+00 | 7,248E-01 |
| 28 | 7,050E-01 | 5,420E-07 | 3,711E-01 | 1,583E+01 |
| 32 | 1,850E+00 | 1,394E+00 | 9,926E-07 | 5,853 |
| 34 | 3,026E-03 | 1,001E-02 | 2,905E-03 | 6,657E-02 |
| 40 | 1,003E-07 | 5,584E-02 | 7,001E-02 | 4,878E-02 |
| 44 | 8,693E-07 | 3,546E-04 | 6,111E-03 | 3,373E-03 |
| 50 | 2,910E-09 | 2,077E-02 | 2,652E-02 | 2,283E-02 |
| 51 | 7,650E-07 | 1,808E-02 | 2,421E-02 | 2,309E-02 |
| 52 | 9,952E-07 | 1,970E-02 | 2,564E-02 | 2,239E-02 |
| 53 | 4,267E-07 | 1,325E-02 | 4,181E-02 | 3,160E-02 |
| 54 | 4,776E-07 | 2,517E-02 | 3,990E-02 | 4,574E-02 |
| 55 | 3,458E-07 | 6,714E-02 | 5,892E-02 | 1,009E-01 |
| 56 | 3,370E-07 | 1,769E-02 | 3,343E-02 | 3,711E-02 |
| 58 | 5,504E-08 | 2,835E-02 | 5,870E-02 | 4,267E-02 |
| 60 | 1,240E-07 | 3,829E-01 | 1,204E-01 | 1,246E-04 |
| 64 | 2,974E-07 | 3,006E-02 | 5,171E-02 | 3,224E-04 |
| 95 | 1,588E-07 | 4,337E-02 | 1,397E-02 | 1,099E-02 |
| 96 | 1,263E-04 | 5,084E-02 | 1,748E-02 | 7,193E-03 |
| 98 | 9,529E-05 | 4,995E-04 | 4,085E-03 | 1,110E-02 |

**Source:** Authors

**Table 4.** Proportionality constants regarding the DAEM with four pseudo-components for m/z signals detected related with the pyrolysis of APH + 1% FeSO$_4$ at a 100 K/min heating rate

| m/z | $c_1$ | $c_2$ | $c_3$ | $c_4$ |
|---|---|---|---|---|
| 12 | 7,774E-07 | 5,769E-01 | 3,691E-01 | 8,162E-02 |
| 14 | 2,458E-07 | 1,917E | 3,587E-01 | 1,971 |
| 16 | 1,830E-07 | 7,087E-03 | 5,504E-01 | 2,162 |
| 17 | 1,739E-06 | 4,934E | 1,134 | 8,902 |
| 18 | 1,007E-05 | 1,816E+01 | 8,453 | 4,014E+01 |
| 28 | 3,953E-07 | 3,185 | 2,866 | 6,740E-01 |
| 32 | 4,660E-01 | 2,545E-01 | 1,649E-07 | 3,016 |
| 34 | 6,479E-08 | 1,563E-02 | 4,466E-04 | 3,253E-02 |
| 40 | 4,538E-07 | 1,503E-01 | 8,201E-02 | 3,152E-01 |
| 44 | 7,678E-06 | 4,174 | 2,958 | 4,253 |
| 50 | 5,237E-08 | 3,332E-02 | 1,433E-02 | 3,581E-02 |
| 51 | 2,871E-07 | 2,081E-02 | 8,129E-03 | 5,866E-02 |
| 52 | 1,321E-08 | 2,399E-02 | 8,875E-03 | 5,640E-02 |
| 53 | 1,187E-07 | 3,023E-02 | 2,094E-02 | 6,537E-02 |
| 54 | 2,888E-07 | 1,870E-02 | 1,912E-02 | 7,988E-02 |
| 55 | 6,239E-08 | 2,523E-02 | 1,166E-02 | 1,722E-01 |
| 56 | 3,994E-04 | 2,605E-02 | 5,213E-03 | 8,258E-02 |
| 58 | 7,451E-04 | 6,835E-02 | 7,989E-07 | 6,423E-02 |
| 60 | 2,261E-07 | 3,386E-01 | 7,752E-02 | 5,932E-02 |
| 64 | 1,177E-03 | 1,029E-01 | 2,436E-08 | 8,370E-02 |
| 95 | 9,348E-08 | 4,438E-02 | 8,566E-03 | 1,231E-02 |
| 96 | 1,557E-07 | 4,771E-02 | 9,458E-03 | 1,521E-02 |
| 98 | 1,150E-07 | 2,171E-03 | 8,642E-04 | 4,755E-03 |

**Source:** Authors

Moreover, in the absence of the catalyst, the fragments associated with the m/z = 14, 32, 34, 50, 64, and 98 were associated with the thermal decomposition of all major biomass components, extractives, hemicellulose, cellulose, and lignin. Similarly, in the presence of the catalyst, m/z = 32 was associated with the thermal decomposition of extractives, hemicellulose, cellulose, and lignin. However, for m/z = 64, the presence of FeSO$_4$ changed the m/z signal intensity profiles, and the evolution of this fragment was only associated with the thermal decomposition of hemicellulose and cellulose. In the presence of FeSO$_4$, m/z = 50, 34, and 98 were associated with the thermal decomposition of hemicellulose, cellulose, and lignin, but not extractives. Finally, the evolution of the fragment of ratio m/z = 14 was associated with the thermal decomposition only of hemicellulose and lignin in the presence of FeSO$_4$. For the aforementioned m/z ratios, in the absence of the catalyst, the peak corresponding to the decomposition rate of cellulose is higher than that corresponding to the decomposition of hemicellulose, which was higher than the peak corresponding to the decomposition of lignin. In contrast, in the presence of the catalyst, the peak corresponding to lignin decomposition is higher than those corresponding to hemicellulose and cellulose decomposition, with the contribution of the thermal decomposition of cellulose being smaller or negligible in some cases, except for m/z = 64 for which the contribution of the thermal decomposition of lignin is negligible.

For all m/z ratios, the catalytic effect of FeSO$_4$ on hemicellulose and lignin can be evidenced as a displacement to the left of the DAEM fit for the thermal decomposition of hemicellulose and lignin: the peaks go from being broad in the absence of the catalyst to becoming narrow in its presence. This means that decomposition occurs at lower temperatures (increasing the decomposition rate), and in a shorter period of time. Additionally, the thermal decomposition of cellulose in the absence of the catalyst occurs in a short period of time and it takes longer in its presence.

## Conclusions

This work studied the effect of FeSO$_4$ on the APH pyrolysis process. It was found that the catalyst mainly affects the thermal decomposition of hemicellulose and lignin and that FeSO$_4$ promotes the formation of compounds for ratios m/z = 64, 95, and 96 –corresponding to fragments of molecules, such as SO$_2$, hydrocarbon ions of general formula $[C_nH_{2n-3}]^+$, and furfural, respectively– due to the iron deoxygenation effect, which improves hydrocarbon formation. The m/z ratios of the gases evolved in the presence of the catalyst were compared with the signals corresponding to its absence. A difference in the formation of peaks shows an effect on the rate of production in the presence of FeSO$_4$, thus increasing the decomposition rate in the case of hemicellulose and lignin, and decreasing it in the case of cellulose.

# References

Albis A., A. R., Muñoz, E. O., Ariza, I. P., Suárez-Escobar, A. F., and Ariza-Barraza, C. S. (2018). TG characterization of pyrolysis of cassava starch residues catalyzed by ferric sulfate. *Contemporary Engineering Sciences*, *11*(72), 3587-3597. https://doi.org/10.12988/ces.2018.87365

Albis, A., Ortiz, E., Piñeres, I., Suárez, A., and Vanegas, M. (2018). Devolatilization of African Palm (*Elaeis guineensis*) Husk studied by TG-MS. *Ingeniería e Investigación*, *38*(2), 9. https://doi.org/10.15446/ing.investig.v38n2.67743

Albis, A., Ortiz, E., Suárez, A., and Piñeres, I. (2014). TG/MS study of the thermal devolatization of Copoazú peels (*Theobroma grandiflorum*). *Journal of Thermal Analysis and Calorimetry*, *115*(1), 275-283. https://doi.org/10.1007/s10973-013-3227-8

Ansari, K. B., and Gaikar, V. G. (2019). Investigating production of hydrocarbon rich bio-oil from grassy biomass using vacuum pyrolysis coupled with online deoxygenation of volatile products over metallic iron. *Renewable Energy*, *130*, 305-318. https://doi.org/10.1016/j.renene.2018.06.052

Bhoi, P. R., Ouedraogo, A. S., Soloiu, V., and Quirino, R. (2020). Recent advances on catalysts for improving hydrocarbon compounds in bio-oil of biomass catalytic pyrolysis. *Renewable and Sustainable Energy Reviews*, *121*, 109676. https://doi.org/10.1016/j.rser.2019.109676

Brassard, P., Godbout, S., Raghavan, V., Palacios, J. H., Grenier, M., and Zegan, D. (2017). The production of engineered biochars in a vertical auger pyrolysis reactor for carbon sequestration. *Energies*, *10*(3), 288. https://doi.org/10.3390/en10030288

Cai, J., Wu, W., and Liu, R. (2014). An overview of distributed activation energy model and its application in the pyrolysis of lignocellulosic biomass. *Renewable and Sustainable Energy Reviews*, *36*, 236-246. https://doi.org/10.1016/j.rser.2014.04.052

Cao, Z., Niu, J., Gu, Y., Zhang, R., Liu, Y., and Luo, L. (2020). Catalytic pyrolysis of rice straw: Screening of various metal salts, metal basic oxide, acidic metal oxide and zeolite catalyst on products yield and characterization. *Journal of Cleaner Production*, *269*, 122079. https://doi.org/10.1016/j.jclepro.2020.122079

Chen, X., Che, Q., Li, S., Liu, Z., Yang, H., Chen, Y., Wang, X., Shao, J., and Chen, H. (2019). Recent developments in lignocellulosic biomass catalytic fast pyrolysis: Strategies for the optimization of bio-oil quality and yield. *Fuel Processing Technology*, *196*, 106180. https://doi.org/10.1016/j.fuproc.2019.106180

Edye, L. A., Richards, G. N., and Zheng, G. (1992). Transition metals as catalysts for pyrolysis and gasification of biomass. In M. Rashid Khan (Ed.), *Clean Energy from Waste and Coal* (pp. 90-101). ACS Publications. https://doi.org/10.1021/bk-1992-0515.ch008

Han, Z., Guo, Z., Zhang, Y., Xiao, X., Xu, Z., and Sun, Y. (2018). Pyrolysis characteristics of biomass impregnated with cadmium, copper and lead: Influence and distribution. *Waste and Biomass Valorization*, *9*(7), 1223-1230. https://doi.org/10.1007/s12649-017-0036-5

Hu, X., and Gholizadeh, M. (2019). Biomass pyrolysis: A review of the process development and challenges from initial researches up to the commercialisation stage. *Journal of Energy Chemistry*, *39*, 109-143. https://doi.org/10.1016/j.jechem.2019.01.024

Kaur, R., Gera, P., Jha, M. K., and Bhaskar, T. (2018). Pyrolysis kinetics and thermodynamic parameters of castor (*Ricinus communis*) residue using thermogravimetric analysis. *Bioresource Technology*, *250*, 422428. https://doi.org/10.1016/j.biortech.2017.11.077

Kelly-Yong, T. L., Lee, K. T., Mohamed, A. R., and Bhatia, S. (2007). Potential of hydrogen from oil palm biomass as a source of renewable energy worldwide. *Energy Policy*, *35*(11), 5692-5701. https://doi.org/10.1016/j.enpol.2007.06.017

Kuehl, D. W., and Rozynov, B. (2003). Chromatographic and mass spectral studies of perfluorooctanesulfonate and three perfluorooctanesulfonamides. *Rapid Communications in Mass Spectrometry, 17*(20), 2364-2369. https://doi.org/10.1002/rcm.1181

Kumar, A., Mylapilli, S. V. P., and Reddy, S. N. (2019). Thermogravimetric and kinetic studies of metal (Ru/Fe) impregnated banana pseudo-stem (*Musa acuminate*). *Bioresource Technology*, *285*, 121318. https://doi.org/10.1016/j.biortech.2019.121318

Malika, A., Jacques, N., Jaafar, E. F., Fatima, B., and Mohammed, A. (2016). Pyrolysis investigation of food wastes by TG-MS-DSC technique. *Biomass Conversion and Biorefinery*, *6*(2), 161-172. https://doi.org/10.1007/s13399-015-0171-9

Mjøs, S. A. (2004). The prediction of fatty acid structure from selected ions in electron impact mass spectra of fatty acid methyl esters. *European Journal of Lipid Science and Technology*, *106*(8), 550-560. https://doi.org/10.1002/ejlt.200401013

Onoja, E., Chandren, S., Abdul Razak, F. I., Mahat, N. A., and Wahab, R. A. (2019). Oil Palm (*Elaeis guineensis*) biomass in Malaysia: The Present and Future Prospects. *Waste and Biomass Valorization*, *10*(8), 2099-2117. https://doi.org/10.1007/s12649-018-0258-1

Rasid, N. S. A., Asadullah, M., Malek, N. H., and Amin, N. A. S. (2020). Fast pyrolysis of oil palm empty fruit bunch in an auger reactor: Bio-oil composition and characteristics. *IOP Conference Series: Materials Science and Engineering*, *736*(3), 1-11. https://doi.org/10.1088/1757-899X/736/3/032021

Rivera-Méndez, Y. D., Rodríguez, D. T., and Romero, H. M. (2017). Carbon footprint of the production of oil palm (*Elaeis guineensis*) fresh fruit bunches in Colombia. *Journal of Cleaner Production*, *149*, 743-750. https://doi.org/10.1016/j.jclepro.2017.02.149

Ro, D., Kim, Y. M., Lee, I. G., Jae, J., Jung, S. C., Kim, S. C., and Park, Y. K. (2018). Bench scale catalytic fast pyrolysis of empty fruit bunches over low cost catalysts and HZSM-5 using a fixed bed reactor. *Journal of Cleaner Production*, *176*, 298-303. https://doi.org/10.1016/j.jclepro.2017.12.075

Salema, A. A., Ting, R. M. W., and Shang, Y. K. (2019). Pyrolysis of blend (oil palm biomass and sawdust) biomass using TG-MS. *Bioresource Technology*, *274*, 439-446. https://doi.org/10.1016/j.biortech.2018.12.014

Shen, D., Zhang, L., Xue, J., Guan, S., Liu, Q., and Xiao, R. (2015). Thermal degradation of xylan-based hemicellulose under oxidative atmosphere. *Carbohydrate Polymers*, *127*, 363-371. https://doi.org/10.1016/j.carbpol.2015.03.067

Tao, F., Song, H., and Chou, L. (2010). Hydrolysis of cellulose by using catalytic amounts of FeCl2 in Ionic liquids. *ChemSusChem*, *3*(11), 1298-1303. https://doi.org/10.1002/cssc.201000184

Yim, S. C., Quitain, A. T., Yusup, S., Sasaki, M., Uemura, Y., and Kida, T. (2017). Metal oxide-catalyzed hydrothermal liquefaction of Malaysian oil palm biomass to bio-oil under supercritical condition. *Journal of Supercritical Fluids*, *120*(Part 2), 384-394. https://doi.org/10.1016/j.supflu.2016.05.044

Zhao, S., Liu, M., Zhao, L., and Lu, J. (2017). Effects of organic and inorganic metal salts on thermogravimetric pyrolysis of biomass components. *Korean Journal of Chemical Engineering*, *34*(12), 3077-3084. https://doi.org/10.1007/s11814-017-0209-8